# On the dependence of static flat seal efficeincy to surface defects.

Yann Ledoux, Didier Lasseux, Hugues Favreliere, Serge Samper, Julien Grandjean

**International Journal of Pressure Vessels and Piping,** 2011, **88**, 518-529DOI: 10.1016/j.ijpvp.2011.06.002

# On the dependence of static flat seal efficiency to surface defects

Y. Ledoux [a], D. Lasseux [b,*], H. Favreliere [b], S. Samper [b], J. Grandjean [a]

[a] *Université de Bordeaux, I2M, UMR CNRS 5295, Esplanade des Arts et Métiers, 33405 Talence Cedex, France*
[b] *Laboratoire SYMME, Polytech'Savoie, BP 80439, 74944 Annecy le Vieux Cedex, France*

A B S T R A C T

We report on the role of the modal content of surface defects on static flat seal efficiency. The configuration under consideration is an annular contact between two surfaces, one holding all the defects, the other being assumed flat and infinitely rigid. The analysis is carried out on synthetic "turned-like" surfaces generated by combinations of the first 50 vibrational eigen modes determined from modal discrete decomposition. The transmissivity of the contact, that fully characterizes the seal efficiency, is computed on the basis of a Reynolds model for incompressible flow. The dependence of the trans-missivity upon the modal content of the surface defects is analyzed on a contact pressure range of common use employing a simplified deformation algorithm. Impact of the defects modal content is investigated statistically through a pair of experimental designs. It is shown that, i) the uncertainty on transmissivity, while considering a series of parts, can be drastically reduced if defect modes are well selected; ii) the transmissivity itself can be very significantly decreased when the defects modal content is conveniently controlled. While clearly indicating that the common surface roughness specification is generally not a relevant one to ensure a required seal performance, this work opens wide perspectives on the seal improvement by surface defects optimization only.

*Keywords:*
Static flat seal
Surface defects
Modal decomposition
Design of experiments

## 1. Introduction

Static sealing performed by direct metal to metal contact is a common design in many industrial applications in particular when severe thermodynamic conditions prohibit the use of rubber seal and was shown to be an efficient design of bolted joints [1]. Such a situation is encountered in assemblies in nuclear power plants, cryotechnic engines, devices for petroleum recovery and turbomachines like helicopter engines to cite some but a few. With the increasing need of reducing fugitive emissions and saving energy, the improvement of such assemblies is a crucial issue. Beyond the management of the assembly [2] tightness efficiency depends on many intrinsic parameters such as the material of the surfaces [3], the contact pressure [4,5] the nature and thermodynamic conditions of the fluid to be sealed, and above all, on the surface defects at many different scales of observation ranging from the sub-micronic scales to body dimension [6–8]. Although these last features are key ones, a thorough characterization of their impact on the contact efficiency and on the associate flow through connected open paths is still at its very beginning. In particular, surface specifications provided on technical drawings are most of the time resulting from pragmatism rather than structured approaches elaborated to fulfill specific seal performance. These specifications are generally restricted to two types of defects, namely form error (*e.g.* flatness, circularity) and arithmetic roughness. However, such specifications are insufficient to correctly assess the geometrical impact of surfaces on the seal performance of an assembly. This was recently proven on the basis of experimental observations showing that defects at intermediate scales (waviness) are of major concern for leakage [9]. In this reference, a simplified reconstruction of a real contact was proposed on the basis of defect measurements at two different scales -roughness and waviness. Numerical predictions of the leak rate dependence on the applied contact pressure were successfully compared to experimental data, confirming the role of waviness.

Clearly, the full control of surface defects at all scales during manufacturing processes is still out of reach. A crucial step toward this end is first a thorough understanding of the complex coupled dynamic behavior of the machine-tool-part system that remains a tricky task and that has been barely addressed in details so far [10–13]. Nevertheless, a detailed investigation on the role of surface defects at all scales on the contact and seal efficiency is equally important in order to help defining the required specifications to be considered during the design. The aim of the present work is to progress toward this goal by presenting an analysis on synthetic surfaces as a preliminary approach before a more

* Corresponding author. Tel.: +33 540 003 421.
E-*mail address*: didier.lasseux@cnrs.fr (D. Lasseux).

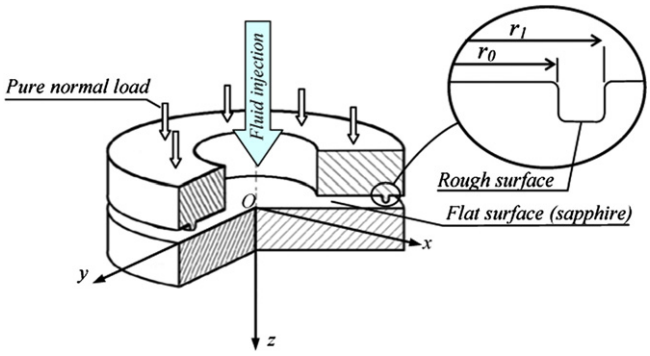


**Fig. 1.** Typical configuration of an annular flat contact.

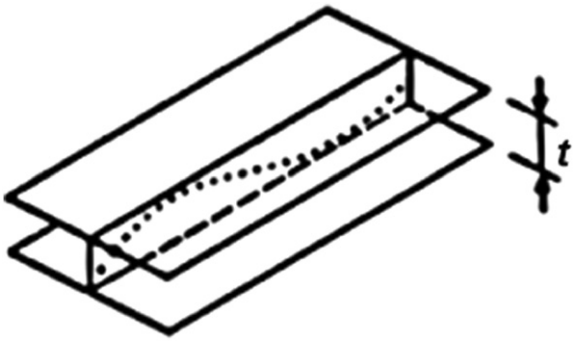


**Fig. 3.** Geometric parameters (from [20]).

thorough study on real parts including leak rate measurements and comparison to numerical predictions.

As a starting point, the analysis is focused on a class of manufactured surfaces obtained by face turning. We assume that the rough surface is annular (inner and outer radii are respectively $r_0$ and $r_1$) and is in contact with a perfectly flat and infinitely rigid surface while a pure normal load is applied. This configuration is a replica of the experimental one used in a former work [14] and is schematically depicted in Fig. 1

The analysis of seal performance is carried out following a procedure summarized on the flow-chart reported in Fig. 2. It consists first in generating synthetic "turned-like" surfaces with the aid of modal discrete decomposition [15]. The procedure allows to monitor the frequency content of surface defects and hence to investigate the potential impact of any defect mode on the leak. This approach is presented in Section 2 of the paper. In a second step, the synthetic surfaces are used as the input for the computation of deformations by the rigid flat plane and flow within the contact. Because a detailed investigation of an adequate deformation model is out of the scope of the present work, we adopt an erosion procedure equivalent to a simplified purely plastic model, keeping in mind that this choice does not introduce any restriction in the overall methodology. The resulting aperture field made of the non-touching zones is used along with the classical Reynolds approximation to compute the transmissivity (i.e. the coefficient

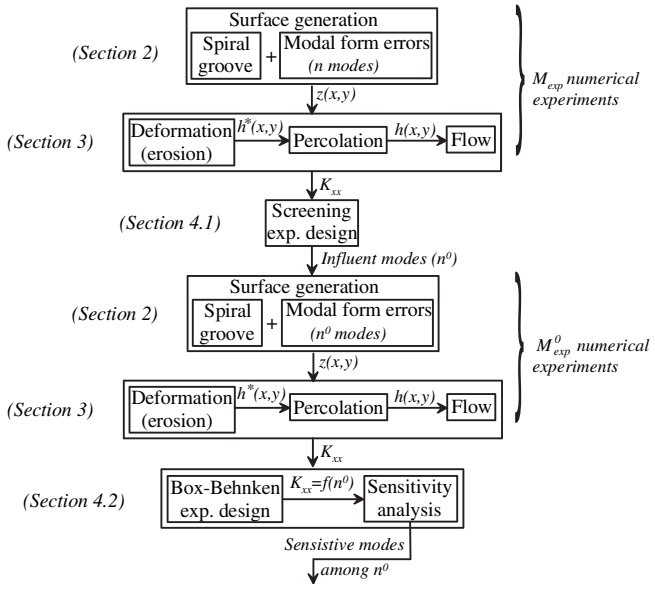


**Fig. 2.** Synoptic of the global methodology.

that linearly relates the flow rate to the pressure gradient) that fully characterizes the seal performance of the annular contact at a given applied load [17,18]. This is detailed in Section 3. In Section 4, the complete procedure is employed to perform an analysis of influential modes on the transmissivity for the class of turned surfaces under consideration. To do so, a statistical approach is followed using two numerical experimental designs. The first one is a Hadamard screening experimental design allowing the identification of statistical modes of the rough surface that are of major impact on the transmissivity. The second one is a quadratic Box-Behnken experimental design that is further used to determine the sensitivity of influential modes yielding recommendations in terms of surface specification to improve seal performance from two different points of view, either in terms of the reduction of transmissivity dispersion on a series of the same part or if a transmissivity minimum is to be achieved.

## 2. Surface defect generation and modal decomposition

The development of the overall method used to assess static flat seal efficiency in relation with surface defects relies on the following hypotheses that were consistently used to design and interpret the experiments detailed in [14]. First, all defects are supposed to be hold by one of the two surfaces only -i.e. the metallic machined annular surface (see Fig. 1)- the other one being perfectly flat. This is consistent with the experimental configuration involving a specular polished sapphire surface that is free of any significant defect in comparison to the machined metallic surface. Alternatively, in a real contact, this hypothesis can be satisfied while making use of the surface-sum concept [19]. Second, the flat surface (the sapphire in the experiment) is supposed to be infinitely rigid. Finally, the relative positioning of the two surfaces is supposed to be ensured by the normal load applied on the flat rigid surface. This means that the rotation of the annular surface about *Ox* and *Oy* axes is free (see Fig. 1) so that the positioning is determined by the *z* translation only. As a consequence surface orientation is not taken into account during the defect generation process which is thus restricted to the representation of form error, waviness and roughness.

The overall surface defects originate from the kinematics and dynamics of the manufacturing process. For face turning, the signature of the kinematics lies in the spiral groove that is basically deterministic. The dynamics gives rise to a series of superimposed defects that are more random in nature, ranging from the material grain scale (roughness) to the scale of the surface itself (form error). As was already highlighted [9] and as will be further confirmed in the present work, the leak is governed by defects of increasing frequency while increasing the contact pressure. Impact of high frequency roughness was analyzed on turned surfaces [16] as well

**Table 1**
Shape parameterization criteria.

| | |
|---|---|
| **Scope:** Ability to represent all classes of surfaces. | **Uniqueness:** Surface is described by a unique set of parameters |
| **Stability:** Parameters variations remain small for small surface changes | **Reversibility:** A given set of parameters yields a unique surface |
| **Efficiency:** Ability to represent a surface with a small number of parameters | **Multi-scale:** Ability to describe surfaces at different scales of observation |
| **Dissociating:** Ability to separate type of geometric errors | **Sensitivity:** Ability to capture small local variation of a surface |
| **Sorting:** Parameters can be sorted in accordance with the surface complexity | **Exhaustivity:** Ability to precisely represent any surface |

as on lapped and sand blasted surfaces that are free of significant waviness using a fractal description [17,18]. Here, the focus is more on the impact of form error and waviness at moderate contact pressures so that roughness of frequency larger than the spiral thread is filtered out of the defect generation. The spiral groove is supposed to have a perfect sinusoidal profile in the radial direction and is superimposed to form error and waviness.

In order to generate realistic form errors and waviness, the parameters defining the geometry and relevant for the subsequent designs of experiment (DOE) must be chosen. The simplest approach would consist in characterizing the deviation from the ideal surface (a plane in our case) by a unique scalar value $t$ representing the maximum amplitude of defects, as shown in Fig. 3 [20]. This approach is of course too simplistic since shape details governing both the contact efficiency (see for instance [21]) and the leak are overlooked. The alternative would be to discretize the surface using a set of points (dotted line in Fig. 3), the parameters being their associated coordinates. This model is very accurate but requires a tremendous number of input data. Intermediate approaches involving a reduced number of parameters and satisfying a set of criteria (see Table 1) as proposed in [22] and later in [23] are thus preferable.

In this context, several approaches can be envisaged like polynomials including Lagrangian interpolations, Bezier splines and surfaces [24] that are often used in computer aided design. However, their scope is poor and they often require surfaces to be split. Moreover, they do not comply with the sorting complexity criterion. Another important class of methods based on periodic decomposition are also widely used. They encompass Fourier series type of

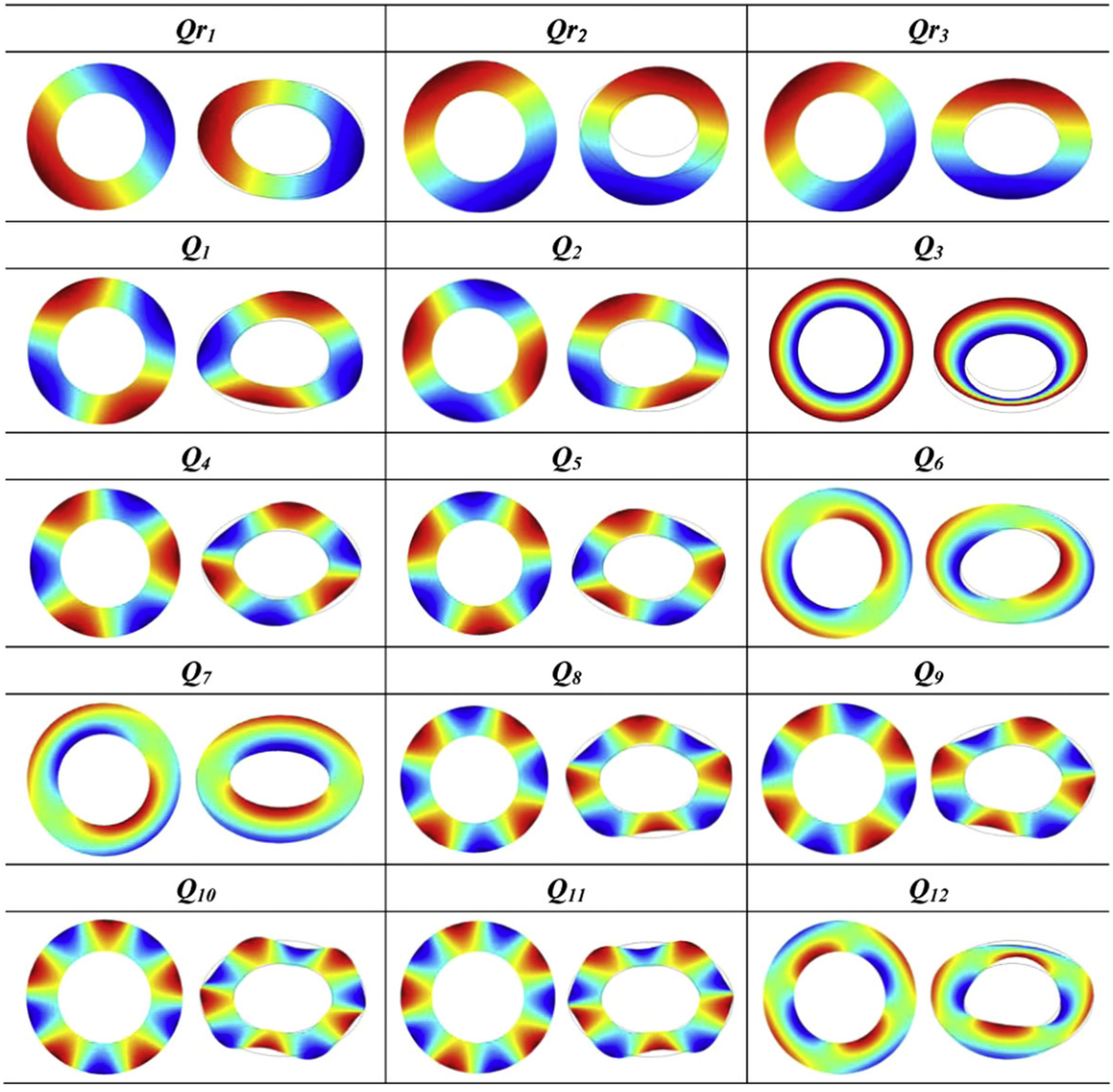


**Fig. 4.** Fifteen first natural modal shapes of an annular surface.

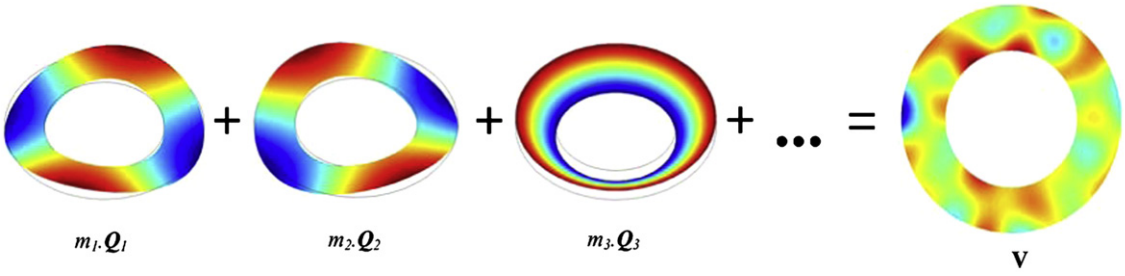


**Fig. 5.** Modal decomposition of form error and waviness.

approach like the discrete cosine transform employed in the case of a stamping process [25], Zernike polynomials [26] used on disk shaped surfaces in optics, Fourier and Chebyshev polynomials employed on cylindrical turned surfaces [27]. These periodic methods have quite all the ten properties of Table 1 except the scope criterion that is not satisfied due to the fact that they implicitly require a description of the form $z(x,y)$. They can however be used on any kind of surface when combined to a segmentation operation.

The Modal Discrete Decomposition (MDD) complies with all of the ten criteria, in particular with the scope, plus a metrics associated to the amplitude of the corresponding mode. This method is used in the present work to generate surface defects.

### 2.1. Modal discrete decomposition (MDD)

The MDD is based on the vibration theory of mechanical structures. Since the eigen- (or natural) vibrational modes provide a variational geometric basis, it is convenient to use them as parameters defining the surface [15,28]. The natural modes can be sorted by increasing frequencies that correspond to modal shapes of increasing complexity (sorting criterion) in accordance with the modal stiffness effect.

To generate form error and waviness using the modal decomposition, the eigen modes of the annular flat surface of inner and outer radii $r_0$ and $r_1$ must be first determined. They are obtained from the solution of the dynamic conservative equilibrium given by

$$\mathbf{M}\cdot\frac{\partial^2\mathbf{u}}{\partial t^2}+\mathbf{K}\cdot\mathbf{u}\ =\ 0 \tag{1}$$

where $\mathbf{M}$ and $\mathbf{K}$ are the mass and stiffness matrices respectively while $\mathbf{u}$ is the displacement vector. This equation, along with the associated boundary conditions that were taken as free displacement at $r = r_0$ and $r = r_1$, is discretized and solved over a grid describing the surface at $N$ discrete points defined in cylindrical coordinates $(r,\theta)$ using for instance a finite element method. In practice, the grid nodal points can be chosen to be exactly the ones that may be used to measure the real manufactured surface if a parallel is to be drawn between the actual surface and an MDD approach.

The solution of Equation (1) provides a linear system which solution yields the eigen modes $\mathbf{Q}_i$ corresponding to the pulsation $\omega_i$ according to

$$\left(\mathbf{M}^{-1}\cdot\mathbf{K}-\frac{1}{\omega_i^2}\mathbf{I}\right)\cdot\mathbf{Q}_i\ =\ 0 \tag{2}$$

where $\mathbf{I}$ is the identity matrix. The first fifteen eigen modes for an annular surface are reported in Fig. 4. Because Equation (1) is solved using free boundary conditions at the inner and outer edges of the annular surface, the three first modes $\mathbf{Q_{r1}}$ to $\mathbf{Q_{r3}}$ (see Fig. 4) refer to rigid body modes corresponding to global displacements of the entire surface. Since these modes are filtered out during the positioning with respect to the flat rigid surface (see discussion above), they are not considered in the rest of the analysis and the nomenclature $\mathbf{Q_i}$ $(i = 1,n)$ to denote the remaining modes is kept in the sequel of the paper. Each eigenvector is normalized according to its infinity norm so that $\|\mathbf{Q_i}\|_\infty\ =\ 1$.

### 2.2. Generation of the synthetic surface using MDD

The annular surface used in the rest of the paper was generated with $r_0 = 19.85$ mm, $r_1 = 20.15$ mm and was discretized with $N = N_r \times N_\theta = 9800$ $(N_r = 71, N_\theta = 140)$ shell elements composed of four nodes. The density, Young modulus and Poisson's ratio of the material were taken as those of 316L stainless steel, namely 7800 kg/m$^3$, 210 GPa and 0.3. Three degrees of freedom -two rotations and one translation- are allowed on each node since bending only is considered. Once the eigen modes $\mathbf{Q_i}$ $(i = 1,n)$ are determined, the annular surface, $\mathbf{V}$, holding form errors and waviness can be decomposed in the corresponding non-orthonormal basis according to (see Fig. 5)

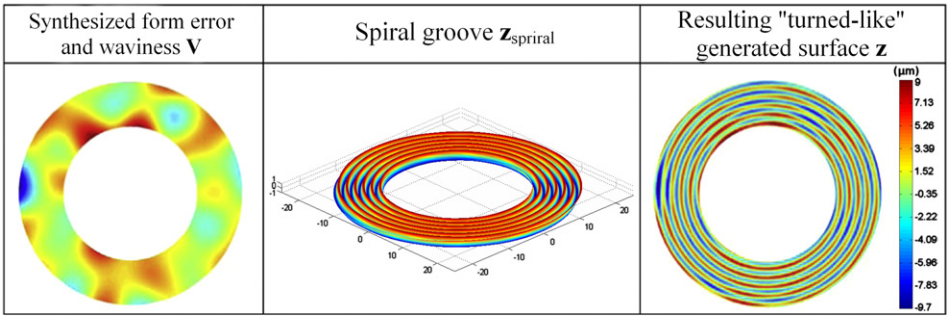


**Fig. 6.** Surface defect generation. The final synthetic surface is $\boldsymbol{z}=\boldsymbol{V}+\boldsymbol{z}_{spiral}$.

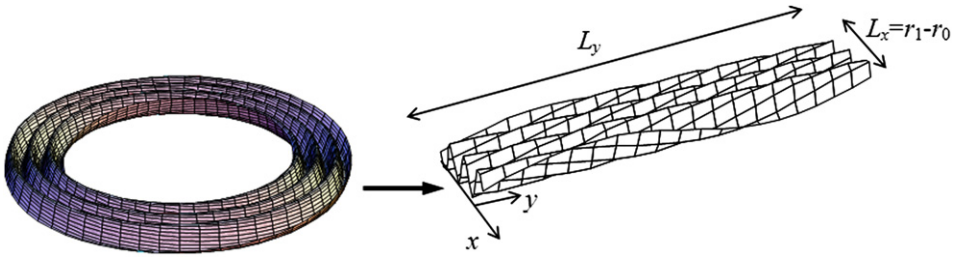


**Fig. 7.** Annular rough surface (left) and the corresponding unrolled strip (right) used in the numerical simulations.

$$\mathbf{V} = \mathbf{Q}\cdot\mathbf{m} \tag{3}$$

**Q** being the $N \times n$ matrix of eigen modes $\boldsymbol{Q_i}$ and **m** the vector of modal coefficients $m_i$ ($i = 1,n$). Since $\boldsymbol{Q_i}$ are unit vectors, a metrics can be attributed to $m_i$. In the following, these coefficients were chosen to have all the same value and were renormalized in the DOE according to a procedure described in Section 4.1.

In accordance with the exhaustivity criterion, any wavy shape for this annular surface can be decomposed with this method, the eigen modes basis being infinite. However, in practice, the number of useful modes remains limited and this limit can be specified by a criterion on the residue with respect to a desired (measured) surface. In the present work, the basis was restricted to $n = 50$. This choice limits the complexity of the analysis while maintaining richness in the description of defects as will be shown in the discussion on the resulting influential parameters on seal efficiency.

The "turned-like" surface, $\boldsymbol{z}$, is finally achieved by superimposing the spiral groove, resulting from the kinematics of the manufacturing process, to $\boldsymbol{V}$. This process is depicted in Fig. 6. The spiral groove shape is given by

$$z_{spiral_i} = A\cos\left(2\pi\frac{r_j}{t}+\theta_k\right) \quad i = j\times k = 1,N \quad j = 1,N_r \quad k = 1,N_\theta \tag{4}$$

where $t$ and $A$ are the pitch and amplitude of the spiral groove that were taken as typical values for a turning process, namely $t = 50$ μm and $A = 20$ μm. The final surface, $z(x = r\cos(\theta), y = r\sin(\theta))$, is hence given at $N$ discrete points according to

$$z_i = V_i + z_{spiral_i} \quad i = 1,N \tag{5}$$

## 3. Transmissivity of the contact

Once the "turned-like" surface is generated, the estimation of the transmissivity of the contact as a function of the applied normal stress can be performed as described in this section. The transmissivity refers to the coefficient that linearly relates the pressure gradient between the contact edges ($r = r_0$ and $r = r_1$) to the macroscopic viscous flow rate.[1] Before detailing the numerical procedure to compute this quantity, the underlying physical model is recalled.

### 3.1. Physical model

The choice of a relevant model of deformation for the contact between rough surfaces remains a tricky task, both from a theoretical and numerical implementation points of view [29,30] and will not be discussed in the present work. The focus is rather on the analysis of the role of the eigen modes on the transmissivity of the contact. As will be shown below with a case example, this requires a great number of simulations and to keep the analysis tractable, a fast algorithm is needed. As a first approach, and for simplification purposes, the model of deformation of the annular generated surface by the perfect rigid plane is an erosion procedure equivalent to a simplified purely plastic model. This choice does not introduce any restriction in the overall methodology. Moreover, it was shown in a previous work [9] that this simplified deformation model is very relevant and yields deformation in complete agreement with more complete elasto-plastic deformation models for turned surfaces.

In the erosion procedure, it is assumed that the normal stress at the surface in effective contact with the flat plane is bounded by the hardness $H$ of the material. We denote $Pca$ the apparent contact pressure given by $Pca = \frac{F}{S}$ where $F$ is the normal force applied to the contact and $S$ the total area of the annular contact of inner and outer radii $r_0$ and $r_1$, $S = \pi(r_1^2 - r_0^2)$. The erosion procedure consists in locating the position of the rigid plane in the direction normal to the mean plane of the surface $z(x,y)$ so that the effective contact area $S_{eff}$ satisfies the force balance given by

$$Pca = H\frac{S_{eff}}{S} \tag{6}$$

The result of the deformation process applied to the original surface $z(x,y)$ is an aperture field $h^*(x,y)$ ($h^*(x,y) = 0$ at actual contact points). This field is further processed using a percolation algorithm to filter out non-percolating clusters, i.e. zones of non-zero aperture that are disconnected from both the inner and outer contact edges. The resulting aperture field, $h(x,y)$, is used to compute the effective transmissivity (see Fig. 2). This is achieved by solving the governing equations of the flow of an incompressible fluid of dynamic viscosity $\mu$ saturating the contact when a pressure difference is applied between the inner (radius $r_0$) and outer (radius $r_1$) edges of the annular contact. The flow is assumed to be slow enough for the Stokes approximation to hold, i.e. inertia and acceleration effects are negligible. Moreover, when asperities on the surface have small slopes (this is always the case for machined surfaces [31]) the Stokes equation can be pre-integrated in the direction normal to the mean plane yielding the following Reynolds model in the continuous form

$$\mathbf{q} = -\frac{h^3}{12\mu}\nabla p \tag{7}$$

$$\nabla\cdot\mathbf{q} = 0 \tag{8}$$

$$\mathbf{q}\cdot\mathbf{n} = 0 \quad \text{on} \quad C_{sf} \tag{9}$$

where $\mathbf{q}$ is the local volume flow rate per unit length ($q_{w_1} = \frac{dQ_{w_1}(x,y)}{dw_2}$ $w_1, w_2 = x, y$ $w_1 \neq w_2$), $Q_{w_1}(x,y)$ being the

[1] This coefficient is sometimes called *permeability* although it has the unit of a cubic length while the permeability has the unit of a square length.

local volume flow rate in the $w_1$ direction) while $C_{sf}$ represents the contours of the effective contact areas. It should be noted that $h^3/12$ represents the local transmissivity. Due to the strong contrast between the width of the contact and its mean radius $2\frac{r_1 - r_0}{r_1 + r_0} << 1$, the problem is solved in cartesian coordinates on a strip of length $L_y = \pi(r_1 + r_0)$ and width $L_x = r_1 - r_0$ (see Fig. 7) with the associated boundary conditions

$$p = P_0 \quad x = 0 \tag{10}$$

$$p = P_1 \quad x = L_x \tag{11}$$

$$p(y = 0) = p(y = L_y) \quad \forall x \tag{12}$$

$$\mathbf{q}(y = 0) = \mathbf{q}(y = L_y) \quad \forall x \tag{13}$$

### 3.2. Estimation of the transmissivity and validation

Equations (7)–(13) correspond to a diffusion-like problem where the local transmissivity $h^3/12$ is a heterogeneous field obtained, in the discrete form, by the procedure described in Section 2. The solution of this problem is achieved numerically. The set of Equations (7)–(13) is discretized making use of a second order finite volume scheme on the grid corresponding to that resulting from the surface generation process. A pre-conditioned conjugate gradient algorithm is employed to solve the linear system. Finally, the computed field $q_x$ is averaged yielding the macroscopic transmissivity $K_{xx}$ of the contact in the $x$ direction according to

$$\langle q_x \rangle = \frac{K_{xx}}{\mu} \frac{P_1 - P_0}{L_x} \tag{14}$$

In the above relationship, $\langle q_x \rangle$ is the superficial average of $q_x$ performed on the total contact area $S$, namely $\langle q_x \rangle = \frac{1}{S}\int_S q_x \mathrm{d}A$. Note that $K_{xx}$ is the key parameter that fully characterizes the seal efficiency of the contact at a given *Pca*.

The numerical procedure described above was applied to estimate the transmissivity that was measured experimentally on a real contact between a 316L stainless steel turned surface (properties are recalled in Section 2) and a flat sapphire as represented in Fig. 1 where $r_0 = 19.85$ mm and $r_1 = 20.15$ mm. The objective of the comparison between the experimental data and the estimation from a reconstructed contact is to validate the physical model and its numerical solution in a real situation.

Liquid leak rates through the contact could be measured for a fluid pressure up to 30 bar and a contact pressure *Pca* ranging from 50 to 700 MPa. The experimental device and protocol used for these measurements are detailed in [14,32]. Using the macroscopic model of Equation (14), the transmissivity $K_{xx}$ can be deduced from leak rate measurements in a straightforward manner. In Fig. 8, we have reported experimental results of $K_{xx}$ versus *Pca* obtained on two different turned surfaces that were machined under the same conditions and referred to as Exp. 1 and Exp. 2 in this figure. These results show that the transmissivity drastically decreases by roughly six orders of magnitude when *Pca* increases from 100 to 700 MPa, following a power law [14]. It should be noted that the two series of measurements performed on the two different surfaces are in very good agreement suggesting a satisfactory reproducibility of the experiment.

To test the ability of the physical model described above to represent experimental observations, simulations were carried out using a simplified representation of the real rough metallic surfaces. This simplified representation was based on a combination of defects recorded on the real surface at two different scales [9]. Defects at the micro scale -basically roughness- were captured from a radial profile on the annulus. The profile was extracted from relief measurement on a small portion of the annular surface using white light interferometry. Macro scale defects -waviness- were recorded in the orthoradial direction by conventional fingering using a flatness measurement device. Results on $K_{xx}$ obtained from this representation of the real surfaces were computed in the same range of *Pca* as the one investigated experimentally. They are represented in Fig. 8.

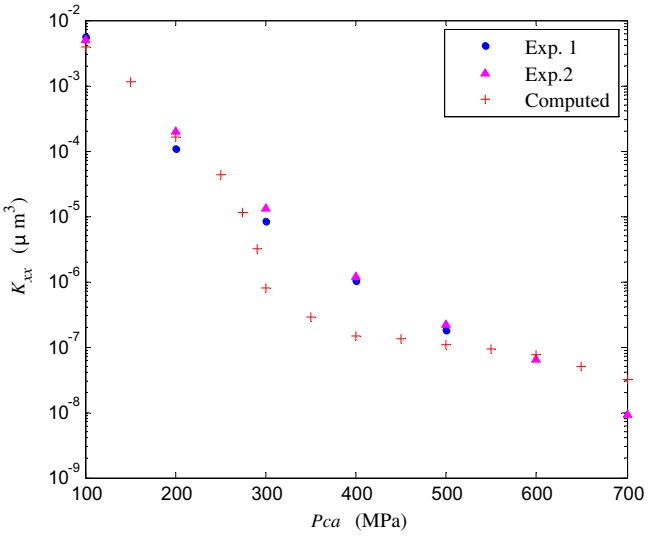


**Fig. 8.** Transmissivity $K_{xx}$ versus the apparent contact pressure Pca. Comparison between numerical estimations and experimental data obtained on two different samples (Exp. 1 and Exp. 2).

Although some discrepancy can be observed in the intermediate range of contact pressure, the overall agreement is satisfactory over the six orders of magnitude variation of $K_{xx}$. The discrepancy is obviously the signature of the oversimplified description of the geometry. Typically, the prediction shows two different leak regimes. At low *Pca*, leakage essentially occurs due to direct flow in the radial direction as a result of waviness that was reproduced on the surface using fingering measurements. At about 250 Mpa, the regime switches from radial to circumferential for which flow mainly occurs through the spiral groove. This is a direct signature of waviness flattening giving predominance to short-scale defects that was reproduced onto the surface using the profile measured by interferometry. This abrupt change results from the simplified two-scale representation of the contact and is not observed experimentally. Indeed, the real topography is evidently much richer in terms of the different scales (wavelengths) involved in the deformation and flow mechanisms, leading to a much smoother dependence of $K_{xx}$ on *Pca* than the predicted one as addressed in [33,34]. The slope difference of $K_{xx}$ between experimental data and numerical prediction at $Pca \geq 450$ MPa suggests that, even in that range of Pca, the pure circumferential leak regime is not yet reached experimentally.

On the basis of this very successful comparison which validates the above model for $K_{xx}$, at least at sufficiently low *Pca* (ranging from 50 MPa to 250 MPa, see below) for which leakage results essentially from waviness of particular interest in the present work, we are in position to use the numerical procedure described above to analyze influential modes on $K_{xx}$ using surfaces generated with the modal decomposition approach detailed in Section 2.

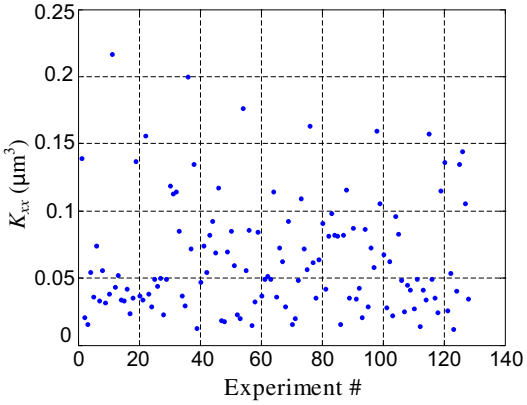


**Fig. 9.** Computed values of $K_{xx}$ versus the experiment number. $Pca = 150$ MPa.

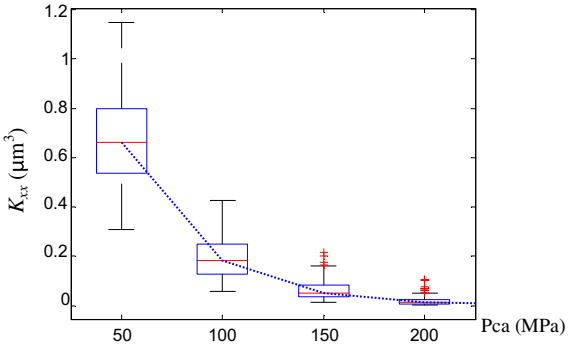


**Fig. 11.** Boxplot representation of the computed values of $K_{xx}$ versus $Pca$.

## 4. Statistical analysis

The objective is now to analyze the influence of the different modal defects on the static seal efficiency of the contact and to rank them by statistical selection in order to derive general trends on static flat seal efficiency. This is performed with surfaces having the properties given in Section 2.2 and $Pca$ in the range 50–200 MPa which is of classical industrial application.

First, a screening approach is used (Section 4.1). This approach allows the identification of the $n^0$ most influential modes among the $n$ modes ($n = 50$) used to generate the surface so that the number of numerical experiments can be reduced (from $M_{exp}$ to $M^0_{exp}$, see Fig. 2). The analysis is then focused on these parameters, i.e. on the modal coefficients $m_i$, $i$ being the number of a mode among the $n^0$ selected ones (see Section 4.2). A quadratic response surface is computed by using a Box-Behnken DOE allowing sensitivities estimation of the $n^0$ modal defects on $K_{xx}$.

### 4.1. Screening design

If every possible surface generated with the 50 first modes with only two different levels is to be tested, this requires $2^{50} \cong 1.12 \times 10^{15}$ combinations, which is totally out of reach. It is thus necessary to use a structured and sequential approach, i.e. a screening strategy, to reduce the number of numerical experiments. Screening can be regarded as a parsimonious approach leading to identify influential parameters among the initial ones with a minimal number of simulations. Different approaches of screening are proposed in the literature like supersaturated design [35] or a usual factorial fractional DOE that can be based on

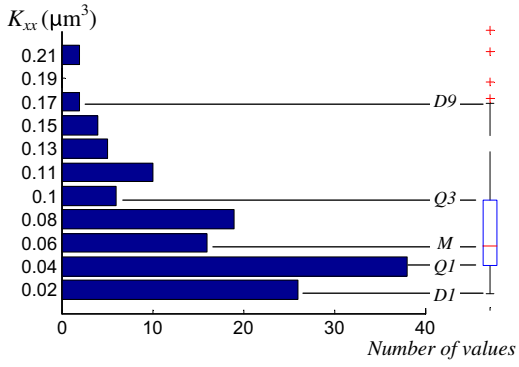


**Fig. 10.** Histogram of the computed values of $K_{xx}$ and determination of the corresponding boxplot. $Pca = 150$ MPa.

Hadamard matrices. The supersaturated design consists in aggregating several variables into one parameter -an alias- and determining the influence of each alias. This technique obviously leads to a number of needed experiments smaller than the initial number of parameters. However, the selection of relevant aliases is a difficult task since some knowledge on influential parameters is required a priori with a risk of overlooking some of them depending on the choice of aggregation [36]. To circumvent such a difficulty, a Hadamard design was used, for which the number of needed experiments is close to the number of parameters to study.

To avoid any statistical bias, a unique metric value $m$ was taken for all the modal coefficients $m_i$, $i = 1, 50$. The Hadamard table was built according to a standard procedure [37]. Each modal coefficient in the table is allowed to take a level $x_i = \pm 1$ (i.e. $m_i = \pm m$, $i = 1, 50$), leading to a set of $M_{exp} = 128$ different experiments, i.e. 128 generated surfaces (see Fig. 2). This number of experiments allows the analysis of the effect of the 50 modes without any alias between modes and their two-way interactions. Each line of the table corresponds to an experiment number characterized by a combination of the 50 modal coefficients taking the value $\pm m$. To be more realistic, the amplitude of all the generated surfaces, each of them being described by a vector $\mathbf{V}$ (see Section 2.2), was renormalized so that the maximum amplitude on the overall set of $\mathbf{V}$ is equal to 20 µm. This value is exactly that of the amplitude $A$ of the spiral groove superimposed to $\mathbf{V}$ as described in Section 2.2. With this choice, both dynamics and kinematics effects of the manufacturing process are comparable. The transmissivity of each of the $M_{exp}$ resulting surfaces $\mathbf{z}$ is computed for $Pca$ ranging from 50 to 200 MPa, every 50 MPa. A screening analysis can hence be performed from this Hadamard DOE by identifying a linear metamodel, $K_{xx\_lin}$, between the computed values of $K_{xx}$ and the modal coefficient levels, $x_i$, for each value of $Pca$ according to

$$K_{xx\_lin} = a_0 + \sum_{i=1}^{n=50} a_i x_i \tag{15}$$

The mean value $a_0$ and the influence coefficients, $a_i$, of the $i$th mode are estimated in the least-squares sense over the $M_{exp}$ numerical experiments. In the framework of the screening analysis, the $K_{xx\_lin}$ model is only valid for the specific combination

**Table 2**
Median and deciles values of $K_{xx}$ for $Pca$ ranging from 50 MPa to 200 MPa.

| $Pca$ (MPa) | 50 | 100 | 150 | 200 |
|---|---|---|---|---|
| $M$ (µm$^3$) | 0.66 | 0.18 | 0.05 | 0.014 |
| $D1$ (µm$^3$) | 1.15 | 0.43 | 0.16 | 0.05 |
| $D9$ (µm$^3$) | 0.31 | 0.06 | 0.012 | 0.003 |
| $K_{xx}$ variation range (µm$^3$) | 0.84 | 0.37 | 0.148 | 0.047 |

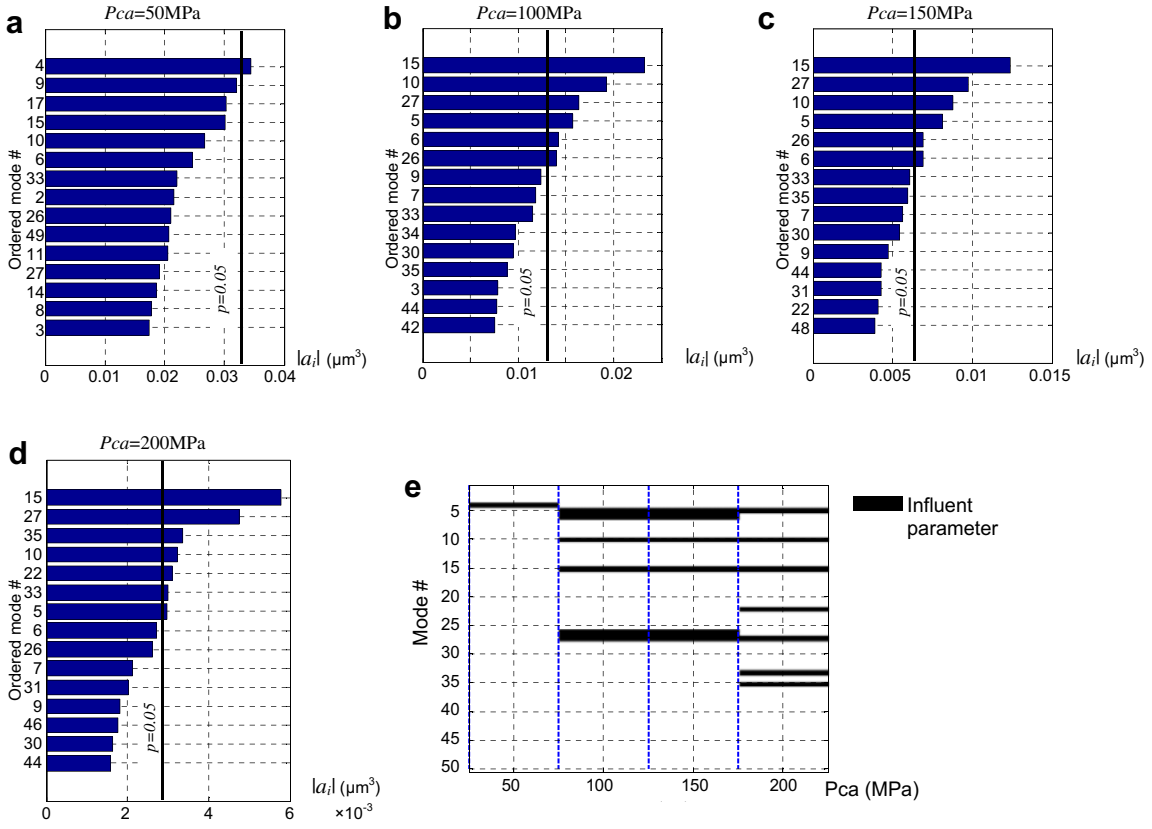


**Fig. 12.** a–d) Ordered absolute values of influence coefficients $a_i$ in the metamodel $K_{xx\_lin}$ (Equation (15)) for Pca in the range 50 MPa–200 MPa. e) Synthesis of statistical influential modes in $K_{xx\_lin}$.

considered in the DOE and should therefore not be used for any interpolation or extrapolation.

In Fig. 9, we have reported the computed values of $K_{xx}$ versus the experiment number for $Pca = 150$ MPa showing that the transmissivity is widely spread as evidenced on the histogram of $K_{xx}$ reported in Fig. 10 for this value of $Pca$. The statistical information on $K_{xx}$ can be synthesized with the boxplot which construction is illustrated in Fig. 10 and that gathers the median value (the red line in the box noted $M$), the first and last quartiles (box bounds noted $Q1$ and $Q3$) and deciles (outgoing dashed lines of the box, $D1$ and $D9$).

Boxplots are represented in Fig. 11 for the whole range of $Pca$. As expected, $K_{xx}$ strongly decreases while increasing Pca, the median value following roughly a power law ($K_{xx} \approx 32345 Pca^{-2.7}$, $R^2 \approx 0.96$), a behavior in accordance with experimental results [14] confirming that the static seal efficiency of the contact can be improved by increasing the contact pressure.

The contact pressure, although fundamental to affect the transmissivity, is however limited in practice by the strength and rigidity of the assembly that do not necessarily allow to apply the load required to achieve a desired level of tightness. Interestingly, a close attention to the above results clearly shows that an alternative to optimize the seal efficiency without modifying the design of the assembly consists in carefully controlling the modal defects of the surface. Indeed, their combinations induce variations of $K_{xx}$ comparable to the median values as clearly highlighted by the different values of $M$ and the variation of $K_{xx}$ corresponding to deciles $D1$ and $D9$ sketched in Fig. 11 and reported in Table 2. For example, for $Pca = 50$ MPa, $M \cong 0.66$ μm$^3$ while the variation D9–D1 due to the modification of the modal defect is around 0.8 μm$^3$.

To identify the most influential modes among the $n = 50$ initial ones, i.e. the significant influence coefficients $a_i$ in the metamodel $K_{xx\_lin}$ of Equation (15), a statistical approach is necessary. This can be performed using Daniel's diagram [38] or Pareto's chart [39] which is based on a comparison of the parameter effects on the residual variance. This last method was used here. The ordered absolute values of influence coefficients are represented in Fig. 12-a, b, c, d where the only fifteen largest ones were kept on each graph for clearness. A significant limit, materialized by the vertical line on the graphs of Fig. 12, is then calculated from the residual variance according to a threshold taken as $p = 0.05$ which is a classical value for this kind of statistical analysis. Influential modes can finally be selected as those whose influence coefficients are larger than the significant limit corresponding to this criterion on $p$.

The significant modes identified for each investigated value of $Pca$ are gathered in Fig. 12 -e showing that only few modes are influential in the metamodel $K_{xx\_lin}$. In fact, there is only one influential defect corresponding to the mode #4 when $Pca \sim 50$ MPa. When $Pca$ is increased up to 150 MPa, more modes are significant, namely modes #5, 6, 10, 15, 26 and 27. For a contact pressure of 200 MPa, modes #6 and 26 are no longer playing any significant role while modes #22, 33 and 35 become influential. This clearly shows that modes of increasing number, corresponding to shapes of increasing complexity, become influential while increasing the contact pressure, a result that is consistent with the experimental and numerical investigation reported in a previous study [9]. It should also be noted that there is no influential mode larger than mode #35 over the range of Pca under consideration. This indicates that the initial choice of $n = 50$ modes to generate surfaces is fully relevant.

On the whole range of $Pca$ under consideration, the number of significant modes, $n^0$, controlling the value and the variability of $K_{xx}$ is equal to 10 (see their representation in Fig. 13) so that a more

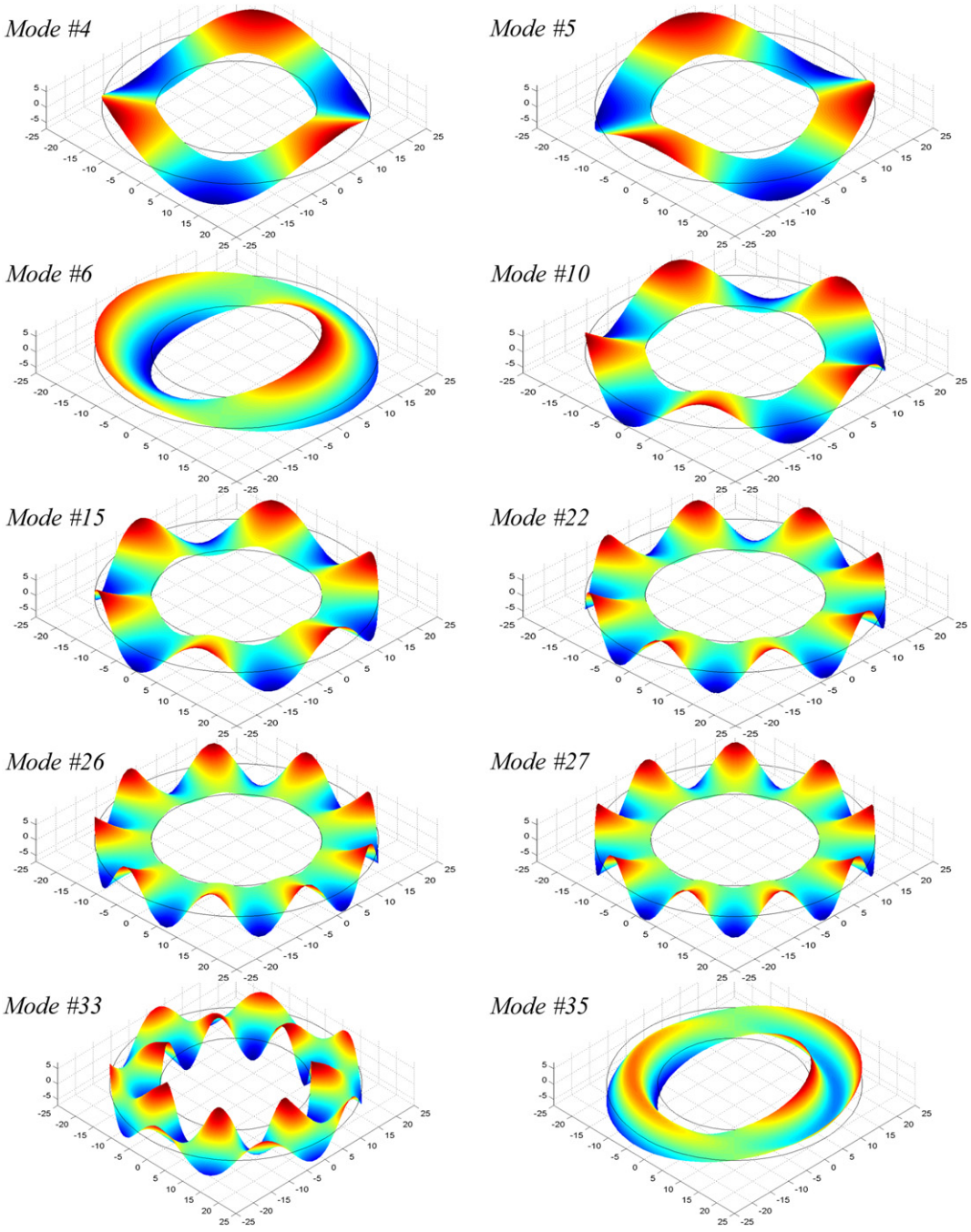


**Fig. 13.** Influential modes for *Pca* ranging from 50 MPa to 200 MPa.

thorough analysis of their respective influence can be performed as proposed in the following section.

### 4.2. Experimental design for response surfaces

A more detailed analysis of the impact of each of the $n^0$ modes over the whole *Pca* range is now performed by making use of an additional DOE composed of $M^0_{\text{exp}}$ experiments (see Fig. 2) to determine a response surface for each value of *Pca*. A Box-Behnken design has been chosen [40] yielding a response surface under the form of a second degree polynomial corresponding to a quadratic model. Each mode $i$ among the $n^0$ modes is allowed to adopt a level $x_i$ having three possible values, namely $-1$, $+1$ and 0, the latter indicating that the mode is extinguished. Experimental points of this DOE are located at the middle of an hypercube (experiments 1 to 160) and are completed by a sequence of 10 central points (experiments 161 to 170) for which all the $n^0$ modes are set to the 0 level. As for the screening design, the DOE, including $M^0_{\text{exp}} = 170$ experiments is repeated for *Pca* ranging from 50 to 200 MPa, every 50 MPa. At each value of *Pca*, the response extracted from this DOE has the form

$$K_{xx\_quad} = b_0 + \sum_i b_i x_i + \sum_i \sum_{j \geq i} b_{ij} x_i x_j \tag{16}$$

where $i$ and $j$ are among the $n^0$ modes {4, 5, 6, 10, 15, 22, 26, 27, 33, 35}. Note that the model in Equation (16) includes the average value

**Table 3**
Response surface accuracy as estimated by $R^2_{adj}$ for *Pca* ranging from 50 MPa to 200 MPa.

| *Pca* (MPa) | 50 | 100 | 150 | 200 |
|---|---|---|---|---|
| $R^2_{adj}$ (%) | 91 | 71 | 60 | 58 |

$b_0$, linear as well as quadratic effects of each mode and interactions between any pair of modes. This model is expected to be predictive for any amplitude of the modes, i.e. for $x_i$ continuously varying on $[-1,+1]$. Hence, the coefficients in Equation (16) were adjusted according to a least-squares procedure constrained by the condition $\min_{x_i,x_j\in[-1,1]}(K_{xx\_quad}) \geq 0$ to keep the model physically realistic out of the points of the DOE. The adjustment quality of the fit was estimated by the adjusted $R^2$ criterion, $R^2_{adj}$, which values are reported in Table 3 for the different values of *Pca*. While decreasing with *Pca* (for *Pca* <100 Mpa), $R^2_{adj}$ remains quasi constant and around 60% in the upper range of the investigated contact pressure, allowing to conclude that the quadratic model $K_{xx\_quad}$ is a relevant one.

As a consequence, the influence of each of the $n^0$ modes on $K_{xx\_quad}$ can now be quantified by determining the sensitivity $\partial K_{xx\_quad}/\partial x_i$ of $K_{xx\_quad}$ to the mode #*i* given by

$$\frac{\partial K_{xx\_quad}}{\partial x_i} = b_i + \sum_{j>i} b_{ij}x_j + \sum_{j<i} b_{ji}x_j + 2b_{ii}x_i \quad i,j\in\{4,5,6,10,15,22,26,27,33,35\} \tag{17}$$

Instead of estimating sensitivities at a specific point of the fitted model which would particularize the conclusion, a more general behavior can be drawn from the dispersion on the sensitivities defined by their maxima and minima respectively expressed as

$$\frac{\partial K_{xx\_quad}}{\partial x_i}\Big|_{\max} = b_i + \sum_{j>i}|b_{ij}| + \sum_{j<i}|b_{ji}| + 2|b_{ii}| \quad i,j\in\{4,5,6,10,15,22,26,27,33,35\} \tag{18}$$

and

$$\frac{\partial K_{xx\_quad}}{\partial x_i}\Big|_{\min} = b_i - \sum_{j>i}|b_{ij}| - \sum_{j<i}|b_{ji}| - 2|b_{ii}| \quad i,j\in\{4,5,6,10,15,22,26,27,33,35\} \tag{19}$$

Dispersions on sensitivities to the $n^0$ modes are represented in Fig. 14 where we have also reported the values of $K_{xx\_quad}$ in µm$^3$ corresponding to the minima and maxima of the sensitivities along with $\max(K_{xx\_quad})$ for each value of *Pca*.

First, sensitivity ranges are relatively well contrasted from one mode to another and are all decreasing with *Pca*. A further conclusive analysis -in a statistical sense- of the effective impact of the different modes on the seal efficiency of the assembly can hence be made. In fact, over the whole *Pca* range, the transmissivity remains weakly sensitive to modes #6, 22, 26 and 27 compared to modes #4, 5, 10, 15, 33 and 35. Among these six important modes,

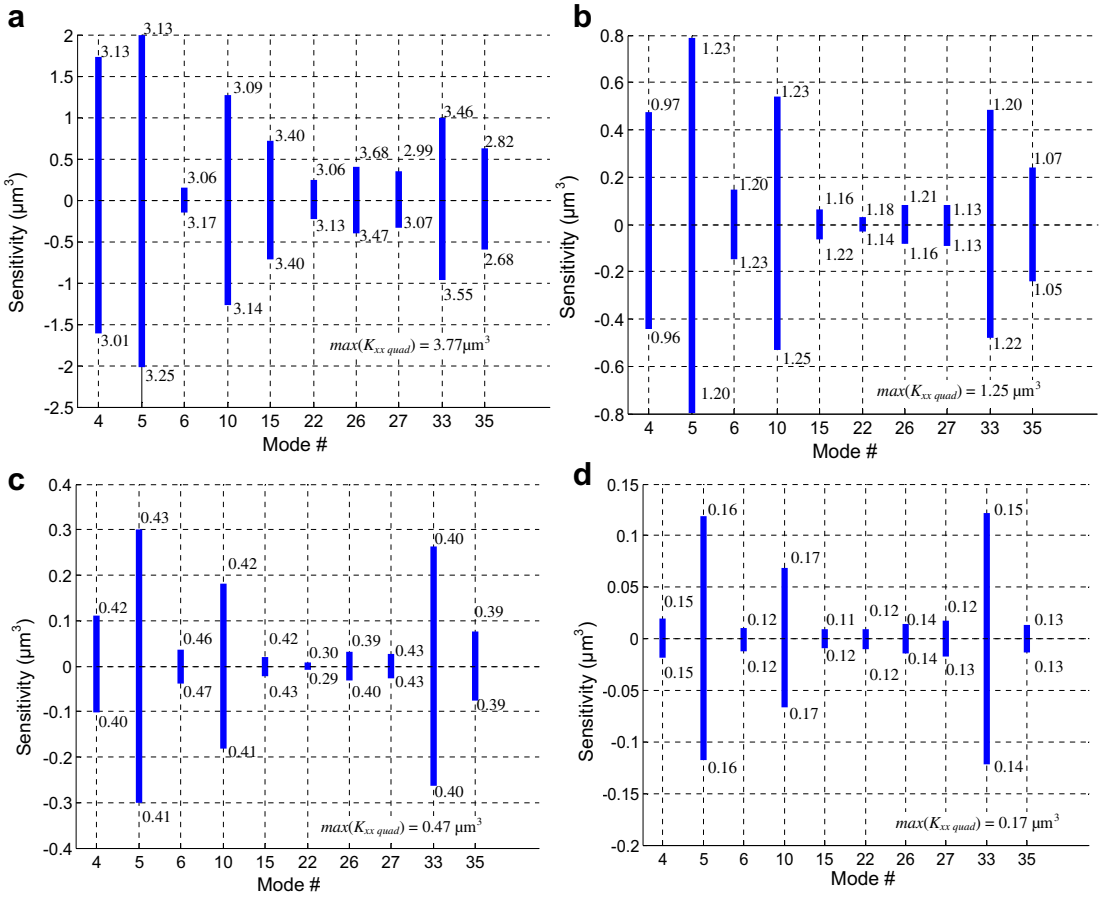


**Fig. 14.** Dispersion on sensitivities of $K_{xx\_quad}$ to the $n^0$ influential modes for a) *Pca* = 50 MPa, b) *Pca* = 100 MPa, c) *Pca* = 150 MPa and c) *Pca* = 200 MPa.

**Table 4**
Level values of the $n^0$ modes yielding $K_{xx}$ minimum for the four values of *Pca* 50, 100, 150, 200 MPa.

| $x_4$ | $x_5$ | $x_6$ | $x_{10}$ | $x_{15}$ | $x_{22}$ | $x_{26}$ | $x_{27}$ | $X_{33}$ | $x_{35}$ |
|---|---|---|---|---|---|---|---|---|---|
| −0.075 | 0.134 | 0.934 | 0.022 | 0.014 | −0.333 | 0.072 | −0.053 | 0.003 | 1 |

however, sensitivity ranges of mode #4, 15 and 35 decrease more rapidly than the three other ones while increasing *Pca*. In particular, modes #4, 15 and 35 would not lead to significant dispersions on the values of $K_{xx}$ if the contact pressure applied to the assembly is large (typically larger than 100 Mpa for mode #15 and 200 MPa for modes #4 and 35). In addition, it must be noted that the values of $K_{xx\_quad}$ corresponding to the minimum and maximum of the sensitivities are close to $\max(K_{xx\_quad})$ for each value of *Pca*. As a consequence, when the surface considered here is taken as a series, a large dispersion on $K_{xx}$ along with a population exhibiting relatively poor seal efficiency are expected when these important modes are present. In other words, a more reliable series would be achieved when an appropriate manufacturing process that does not induce those modes is chosen to machine the surface.

As a different prospect, it is also interesting to investigate the modal content of the surface that would lead to values of $K_{xx}$ close to its minimum. As can be seen from Table 4 gathering the values of the $x_i$ ($i$ being one of the $n^0$ modes) that minimize $K_{xx}$ for the four values of Pca 50, 100, 150 and 200 MPa, all the $x_i$ are small except $x_6$ and $x_{35}$ that are close or equal to the maximum (+1).

Setting all the $x_i$ to 0, except the latter two that are kept to +1, yields values of $K_{xx}$ that are between ∼25 and ∼200 times smaller than the maximum values of $K_{xx}$, $\max(K_{xx\_quad})$, reported in Fig. 14 for the four values of Pca. For this set of mode levels, the corresponding sensitivities remain also much smaller (by a factor ∼1.5 to ∼600) than the maximum (or minimum) values of $\partial K_{xx\_quad}/\partial x_i$ ($i$ being one of the $n^0$ modes) reported in Fig. 14 for the four values of Pca. This indicates that among all the $n^0$ modes, modes #6 and 35 (see Fig. 14 for their illustrations) are in favor of a decreasing transmissivity compared to the other modes. This clearly highlights that the transmissivity can be significantly improved when an appropriate modal content of the surface defects is considered.

## 5. Conclusion

The efficiency of static flat seal resulting from the tight contact between two rough surfaces that is a major issue for many industrial applications involving severe operating conditions (high pressure and/or temperature, cryotechnic conditions, fluid contaminants etc.) was addressed in this work from the point of view of the impact of surface defects. A methodology consisting of decomposing the surface on a vibrational eigen modes basis was employed in order to synthesize "turned-like" surfaces on which transmissivities were computed. This was achieved by solving the flow problem over the whole contact using the Reynolds model, the procedure being validated by experimental data. Due to the number of modes under consideration, a statistical analysis was further used, consisting in a pair of experimental designs, in order to identify the impact of the most significant modes on the transmissivity.

Far beyond the illustrative example of "turned-like" surfaces on which the overall methodology was employed, major conclusions emerge from this analysis. While surface specifications for static flat seal on technical drawings are commonly in terms of roughness and form error, it was clearly highlighted that this is not the optimal requirement in general, except may be when the assembly allow large enough loads to compensate these defects. The present work shows that an appropriate selection of defects modes can be made allowing a drastic reduction of the uncertainty on the transmissivity considering a series of parts, i.e. an improved qualification of seal efficiency. It has also been demonstrated that the transmissivity itself can be very significantly reduced when the modal content of the surface is conveniently controlled. Although the full control of the selected modes that are required to achieve such an improvement is not yet within reach in terms of surface manufacturing, this represents a very promising route for seal improvement since it does not induce any constrain on the design of the assembly itself, the gain being achieved without increasing the applied load.

The methodology and results presented in this paper open very wide perspectives. A short term extension of the work consists in identifying the modal content of a series of surfaces obtained with the same manufacturing process but under different operating conditions. Once sorted according to the modal content of their defects (this can be identified from surface measurement at different scales), a comparison of their transmissivities could be performed both from a direct numerical estimation and from experimental leak rate measurements. Longer term efforts must be dedicated to the understanding of the complex coupled dynamic behavior of the machine-tool-part system and its relationship with the resulting defects on the surface under concern. The useful design guidance for optimal surface specification of static flat seal provided by the development of the present work will be then under control and will orientate the choice of the appropriate manufacturing process.

## Acknowledgments

Support from EDF R&D, the CNES, SNECMA, TURBOMECA, the Aquitaine Region and the CNRS is gratefully acknowledged.

## References

[1] Abid M, Nash DH. Comparative study of the behaviour of conventional gasketed and compact non-gasketed flanged pipe joints under bolt up and operating conditions. Int J Press Vessels Pip 2003;80:831–41.
[2] Sears G, King D. Joint integrity management of critical flanges. Int J Press Vessels Pip 2004;81:513–9.
[3] Yanagisawa T, Sanada M, Koga T, Hirabayashi H. Fundamental study of the sealing performance of a C-shaped metal seal, 2nd International Symposium on Fluid Sealing, La Baule, France; 18–20 September, 1990. 389–398.
[4] Yanagisawa T, Sanada M, Koga T, Hirabayashi H. The influence of designing factors on the sealing performance of C-seal. SAE Trans 1991;100(6):651–7.
[5] Murtagian GR, Fanelli V, Villasante JA, Johnson DH, Ernst HA. Scalability of stationary metal-to-metal seals. J Tribol 2004;126:591–6.
[6] Arghavani J, Derenne M, Marchand L. Effect of surface characteristics on compressive stress and leakage rate in gasketed flanged joints. Int J Adv Manuf Technol 2003;21:713–32.
[7] Lee NKS, Yu G, Joneja A, Ceglarek D. The modeling and analysis of a butting assembly in the presence of workpiece surface roughness and part dimensional error. Int J Adv Manuf Technol 2006;31:528–38.
[8] Abid M, Nash DH. A parametric study of metal-to-metal contact flanges with optimised geometry for safe stress and no-leak conditions. Int J Press Vessels Pip 2004;81:67–74.
[9] Marie C, Lasseux D, Zahouani H, Sainsot P. An integrated approach to characterize liquid leakage through metal contact seal. Eur J Mech Env Eng 2003; 48(2):81–6.
[10] Lin SC, Chang MF. A study on the effects of vibrations on the surface finish using a surface topography simulation model for turning. Int J Mach Tools Manuf 1998;38(7):763–82.
[11] Larue A, Anselmetti B. A prediction of the machining defects in flank milling. Int J Mach Tools Manuf 2004;24:102–11.
[12] Manna A, Bhattacharyya B. Investigation for optimal parametric combination for achieving better surface finish during turning of Al /SiC-MMC. Int J Adv Manuf Technol 2004;23:658–65.
[13] Waikar RA, Guo YB. A comprehensive characterization of 3D surface topography induced by hard turning versus grinding. J Mater Process Technol 2008; 197:189–99.
[14] Marie C, Lasseux D. Experimental leak-rate measurement through a static metal seal. J Fluids Eng 2007;129(6):799–805.
[15] Samper S, Formosa F. Form defects tolerancing by natural modes analysis. J Comput Inf Sci Eng 2007;7(1):44–51.

[16] Robbe-Valloire F, Prat M. A model for face-turned surface microgeometry. Application to the analysis of metallic static seals. Wear 2008;264:980–9.
[17] Vallet C, Lasseux D, Sainsot P, Zahouani H. Real versus synthesized fractal surfaces: contact mechanics and transport properties. Tribol Int 2009a;42: 250–9.
[18] Vallet C, Lasseux D, Sainsot P, Zahouani H. Sampling effect on contact and transport properties between fractal surfaces. Tribol Int 2009b;42:1132–45.
[19] Greenwood J, Williamson J. Contact of nominally flat surfaces. Proc R Soc London Ser A 1966;295(1442):300–19.
[20] ISO 1101. Technical drawings - geometrical tolerancing - tolerancing of form, orientation, location and run-out - generalities, definitions, symbols, indications on drawings. International Organization for Standardization; 1983.
[21] Dong WP, Sullivan PJ, Stout KJ. Comprehensive study of parameters for characterising three dimensional surface topography III: parameters for characterising amplitude and some functional properties. Wear 1994;178:29–43.
[22] Mokhtarian F, Mackworth AK. A theory of multiscale, curvature-based shape representation for planar curves. IEEE Trans Pattern Anal Mach Intell 1992; 14(8):789–805.
[23] Iyer N, Jayanti S, Lou K, Kalyanaraman Y, Ramani K. Three-dimensional shape searching: state-of-the-art review and future trends. Comput-Aided Des 2005;37(5):509–30.
[24] Gupta S, Turner JU. Variational solid modeling for tolerance analysis. IEEE Comput Graphics Appl 1993;13(3):64–74.
[25] Huang W, Ceglarek D. Mode-based decomposition of part form error by discrete-cosine-transform with implementation to assembly and stamping system with compliant parts. CIRP Ann 2002;51:21–6.
[26] ISO 10110-5. Optics and optical instruments - preparation of drawings for optical elements and systems - Part 5: surface form tolerances. International Organization for Standardization; 1996.
[27] Henke RP, Summerhays KD, Baldwin JM, Cassou RM, Brown CW. Methods for evaluation of systematic geometric deviations in machined parts and their relationships to process variables. Precis Eng 1999;23:273–92.
[28] Huang Q-X, Wicke M, Adams B, Guibas L. Shape decomposition using modal analysis. Eurographics 2009;28(2). 30 March-3 April, Munich, Germany, 2009.
[29] Hyun S, Pei L, Molinari JF, Robbins MO. Finite-element analysis of contact between elastic self-affine surfaces. Phys Rev E 2004;70:026117.
[30] Pei L, Hyun S, Molinari JF, Robbins MO. Finite-element modeling of elasto-plastic contact between rough surfaces. J Mech Phys Solids 2005;53:2385–409.
[31] Dowson D. History of tribology. London: Professional Engineering Publishers; 1998.
[32] Lasseux D, Marie C. Apparatus for measuring the amount of leakage of a sealed arrangement. Patent EP1336831; 2008.
[33] Persson BNJ, Yang C. Theory of the leak-rate of seals. J Phys-Condens Matter 2008;20:315011 (11pp).
[34] Bottiglione F, Carbone G, Mangialardi L, Mantriota G. Leakage mechanism in flat seals. J Appl Phys 2009;106:104902.
[35] Lin DKJ. Generating systematic supersaturated designs. Technometrics 1995; 37:213–25.
[36] Abraham B, Chipman H, Vijayan K. Some risks in the construction and analysis of supersaturated designs. Technometrics 1999;41(2):135–41.
[37] Plackett RL, Burman JP. Design of optimum multifactorial experiments. Biometrika 1946;33:305–25.
[38] Box GEP, Hunter WG, Hunter JS. Statistics for experimenters. New York: Wiley; 1978.
[39] Draper N, Smith H. Applied regression analysis. New York: Wiley-Interscience; 1981 (pp. 177–182).
[40] Box G, Behnken D. Some new three level designs for the study of quantitative variables. Technometrics 1960;2:455–75.